

AD-A235 885



DTIC  
ELECTE  
MAY 1 5 1991  
S C D

2

OFFICE OF NAVAL RESEARCH

Contract N00014-89-J-1497

R&T Code 413050. . .02

Technical Report No. 19

$B+(^1S) + H_2 \rightarrow BH+(^2\Sigma) + H$   
A Woodward-Hoffmann Forbidden Ion-Molecule Reaction

by  
Jeff Nichols, Samuel J. Cole, Maciej Gutowski, and Jack Simons

Prepared for Publication in  
The Journal of Physical Chemistry

The University of Utah  
Department of Chemistry  
Salt Lake City, Utah 84112-1194

April 1991



|                    |                                     |
|--------------------|-------------------------------------|
| Accession For      |                                     |
| NTIS GRA&I         | <input checked="" type="checkbox"/> |
| DTIC TAB           | <input type="checkbox"/>            |
| Unannounced        | <input type="checkbox"/>            |
| Justification      |                                     |
| By                 |                                     |
| Distribution       |                                     |
| Availability Codes |                                     |
| Dist               | Avail and/or Special                |
| A-1                |                                     |

Reproduction in whole or in part is permitted for any purpose of the United States Government

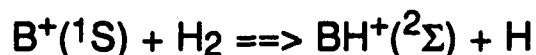
This document has been approved for public release and sale; its distribution is unlimited.



01 5 14 048

## REPORT DOCUMENTATION PAGE

|  |   |  |                         |
|--|---|--|-------------------------|
| 1a. REPORT SECURITY CLASSIFICATION<br>UNCLASSIFIED   |   | 1b. RESTRICTIVE MARKINGS   |                         |
| 2a. SECURITY CLASSIFICATION AUTHORITY  |   | 3. DISTRIBUTION / AVAILABILITY OF REPORT<br>APPROVED FOR PUBLIC RELEASE:<br>DISTRIBUTION UNLIMITED |                         |
| 2b. DECLASSIFICATION / DOWNGRADING SCHEDULE  |   |  |                         |
| 4. PERFORMING ORGANIZATION REPORT NUMBER(S)<br>ONR TECHNICAL REPORT # 19   |   | 5. MONITORING ORGANIZATION REPORT NUMBER(S)  |                         |
| 6a. NAME OF PERFORMING ORGANIZATION<br>THE UNIVERSITY OF UTAH  | 6b. OFFICE SYMBOL<br>(if applicable)        | 7a. NAME OF MONITORING ORGANIZATION<br>OFFICE OF NAVAL RESEARCH<br>CHEMISTRY PROGRAM               |                         |
| 6c. ADDRESS (City, State, and ZIP Code)<br>DEPARTMENT OF CHEMISTRY<br>UNIVERSITY OF UTAH<br>SALT LAKE CITY, UT 84112   |   | 7b. ADDRESS (City, State, and ZIP Code)<br>800 NO. QUINCY ST.<br>ARLINGTON, VA 22217-5000          |                         |
| 8a. NAME OF FUNDING / SPONSORING ORGANIZATION<br>OFFICE OF NAVAL RESEARCH  | 8b. OFFICE SYMBOL<br>(if applicable)<br>ONR | 9. PROCUREMENT INSTRUMENT IDENTIFICATION NUMBER<br>N00014-89-J-1497                                |                         |
| 8c. ADDRESS (City, State, and ZIP Code)<br>800 NO. QUINCY ST.<br>ARLINGTON, VA 22217   |   | 10. SOURCE OF FUNDING NUMBERS  |                         |
|  |   | PROGRAM ELEMENT NO.  | PROJECT NO.             |
|  |   | TASK NO.   | WORK UNIT ACCESSION NO. |
| 11. TITLE (Include Security Classification)<br>B + ( <sup>1</sup> S) + H <sub>2</sub> - BH <sup>+</sup> ( <sup>2</sup> Sigma) + H A Woodward-Hoffmann Forbidden Ion-Molecule Reaction  |   |  |                         |
| 12. PERSONAL AUTHOR(S)<br>Jeff Nichols, Samuel J. Cole, Maciej Gutowski, and Jack Simons   |   |  |                         |
| 13a. TYPE OF REPORT<br>TECHNICAL   | 13b. TIME COVERED<br>FROM 12/90 to 3/91     | 14. DATE OF REPORT (Year, Month, Day)<br>April 17, 1991  | 15. PAGE COUNT          |
| 16. SUPPLEMENTARY NOTATION   |   |  |                         |
| 17. COSATI CODES   |   | 18. SUBJECT TERMS (Continue on reverse if necessary and identify by block number)                  |                         |
| FIELD  | GROUP                                       | SUB-GROUP  |                         |
|  |   |  |                         |
| 19. ABSTRACT<br>The reaction of B <sup>+</sup> ( <sup>1</sup> S) with H <sub>2</sub> on the ground potential energy surface is examined using <i>ab initio</i> electronic structure methods. A weakly bound T-shaped B <sup>+</sup> ...H <sub>2</sub> complex of C <sub>2v</sub> symmetry is found to lie 855 cm <sup>-1</sup> below the B <sup>+</sup> + H <sub>2</sub> reactant energy. Its H-H internuclear distance is only slightly distorted from that of H <sub>2</sub> ; the B-H distance (ca. 2.6 Å) is much longer than the covalent bond length in BH <sup>+</sup> (1.2 Å). Further along the reaction coordinate is found a narrow 'entrance valley' characterized by strong B <sup>+</sup> -to-H <sub>2</sub> inter-reactant forces but very small distortion of the H-H bond length or the H-H vibrational frequency. As one proceeds further up this valley, a geometry is reached at which the asymmetric distortion mode (of b <sub>2</sub> symmetry) develops negative curvature. Distortion along the asymmetric mode leads to a transition state of C <sub>s</sub> symmetry possessing one 'long' B-H distance (r <sub>BH</sub> = 1.765 Å), one 'short' B-H distance (r <sub>BH</sub> ' = 1.251 Å) and an essentially 'broken' H-H bond (r <sub>HH</sub> = 1.516 Å). Its energy lies 22,528 cm <sup>-1</sup> above B <sup>+</sup> + H <sub>2</sub> and 2031 cm <sup>-1</sup> or ca. 0.25 eV above the thermodynamic reaction threshold for BH <sup>+</sup> + H formation, which is predicted to be endoergic by 20,497 cm <sup>-1</sup> . A geometrically stable linear HBH <sup>+</sup> ( <sup>1</sup> Σ) species is found to lie 19,259 cm <sup>-1</sup> below B <sup>+</sup> + H <sub>2</sub> . Its BH bond length (r <sub>BH</sub> = 1.173 Å) is only slightly longer than that in BH <sup>+</sup> (1.2 Å). Similarities and differences among reactions of the isoelectronic Be, B <sup>+</sup> , and Li <sup>+</sup> with H <sub>2</sub> are also discussed. |   |  |                         |
| 20. DISTRIBUTION / AVAILABILITY OF ABSTRACT<br><input checked="" type="checkbox"/> UNCLASSIFIED / UNLIMITED <input type="checkbox"/> SAME AS RPT <input type="checkbox"/> DTIC USERS   |   | 21. ABSTRACT SECURITY CLASSIFICATION<br>UNCLASSIFIED   |                         |
| 22a. NAME OF RESPONSIBLE INDIVIDUAL<br>PROFESSOR JACK SIMONS   |   | 22b. TELEPHONE (Include Area Code)<br>(801) 581-8023   | 22c. OFFICE SYMBOL      |



## A Woodward-Hoffmann Forbidden Ion-Molecule Reaction

Jeff Nichols#, Samuel J. Cole+, Maciej Gutowski, and Jack Simons  
Chemistry Department  
University of Utah  
Salt Lake City, Utah 84112

### Abstract

The reaction of  $\text{B}^+(^1\text{S})$  with  $\text{H}_2$  on the ground potential energy surface is examined using *ab initio* electronic structure methods. A weakly bound T-shaped  $\text{B}^+\cdots\text{H}_2$  complex of  $\text{C}_{2v}$  symmetry is found to lie  $855 \text{ cm}^{-1}$  below the  $\text{B}^+ + \text{H}_2$  reactant energy. Its H-H internuclear distance is only slightly distorted from that of  $\text{H}_2$ ; the B-H distance (ca.  $2.6 \text{ \AA}$ ) is much longer than the covalent bond length in  $\text{BH}^+$  ( $1.2 \text{ \AA}$ ). Further along the reaction coordinate is found a narrow 'entrance valley' characterized by strong  $\text{B}^+$ -to- $\text{H}_2$  inter-reactant forces but very small distortion of the H-H bond length or the H-H vibrational frequency. As one proceeds further up this valley, a geometry is reached at which the asymmetric distortion mode (of  $b_2$  symmetry) develops negative curvature. Distortion along the asymmetric mode leads to a transition state of  $\text{C}_s$  symmetry possessing one 'long' B-H distance ( $r_{\text{BH}} = 1.765 \text{ \AA}$ ), one 'short' B-H distance ( $r_{\text{BH}} = 1.251 \text{ \AA}$ ) and an essentially 'broken' H-H bond ( $r_{\text{HH}} = 1.516 \text{ \AA}$ ). Its energy lies  $22,528 \text{ cm}^{-1}$  above  $\text{B}^+ + \text{H}_2$  and  $2031 \text{ cm}^{-1}$  or ca.  $0.25 \text{ eV}$  above the thermodynamic reaction threshold for  $\text{BH}^+ + \text{H}$  formation, which is predicted to be endoergic by  $20,497 \text{ cm}^{-1}$ . A geometrically stable linear  $\text{HBH}^+(^1\Sigma)$  species is found to lie  $19,259 \text{ cm}^{-1}$  below  $\text{B}^+ + \text{H}_2$ . Its BH bond length ( $r_{\text{BH}} = 1.173 \text{ \AA}$ ) is only slightly longer than that in  $\text{BH}^+$  ( $1.2 \text{ \AA}$ ). Similarities and differences among reactions of the isoelectronic Be,  $\text{B}^+$ , and  $\text{Li}^-$  with  $\text{H}_2$  are also discussed.

#Utah Supercomputer Institute/IBM Corporation Partnership, Salt Lake City, Utah  
84112

Permanent address: CAChe<sup>TM</sup> Group, Tektronix, Inc., P.O. Box 500 M.S. 13-400,  
Beaverton, OR 97077.

~~91 5 14 045~~

## I. Introduction

Earlier theoretical calculations<sup>1</sup> on  $\text{Be}(^1\text{S}) + \text{H}_2 \Rightarrow \text{HBeH}(^1\Sigma)$  and on  $\text{Mg}(^1\text{S}) + \text{H}_2 \Rightarrow \text{HMgH}(^1\Sigma)$  yielded qualitatively similar ground-state,  $\text{C}_{2v}$ -constrained potential energy surfaces. A two-dimensional contour characterization of such  $\text{C}_{2v}$ -constrained potential energy surfaces is given in Fig. 1. Both of these alkaline earth atoms, as well as the analogous  $\text{B}^+$  ion considered here, have  $ns^2\ ^1\text{S}$  ground electronic states and relatively low-lying  $nsnp\ ^1,3\text{P}$  excited states. As discussed in detail below, the chemical reactivity of the  $^1\text{S}$  ground-states of such species is strongly influenced by the presence of the excited  $^1,3\text{P}$  states. Before discussing our motivations for undertaking the theoretical study of the  $\text{B}^+(^1\text{S}) + \text{H}_2 \Rightarrow \text{BH}^+(^2\Sigma) + \text{H}$  reaction and our findings, let us exploit our experience on the Be and Mg reactions to anticipate some of the electronic structure characteristics that would be expected to affect strongly the dynamics<sup>3a,3b,3c</sup> (e.g., energy threshold, cross-section magnitude, and energy dependence) of the  $\text{B}^+ + \text{H}_2$  reaction.

### A. The Electronic Configurations of Interest in $\text{C}_{2v}$ Symmetry

#### 1. The $\text{M} + \text{H}_2$ Reactant and $\text{MH}$ Product Configurations

Briefly, the  $ns^2$  configuration of the reactant M atom (or ion) when combined with the  $\sigma_g^2$  configuration of the  $\text{H}_2$  molecule in its  $X\ ^1\Sigma_g$  ground state, does not correlate with the ground-state  $\sigma_g^2\ \sigma_u^2$  configuration of the linear  $\text{MH}$  molecule (or ion). In  $\text{C}_{2v}$  symmetry, the  $\text{M} + \text{H}_2$  reactants have the  $ns^2\ \sigma_g^2 = 1a_1^2 2a_1^2$  electronic configuration, and the  $\text{MH}$  products have the  $\sigma_g^2\ \sigma_u^2 = 1a_1^2 1b_2^2$  configuration. Moreover, neither of these two configurations can describe the  $\text{MH} + \text{H}$  products which require an 'open-shell' configuration of the form  $\sigma_{\text{MH}}^2\ \sigma_{\text{M}}\ \sigma_{\text{H}}$ . For the  $\text{M} + \text{H}_2$  reactants, the labels  $1a_1$ ,  $2a_1$ , and  $1b_2$  are used to denote the valence M  $ns$ ,  $\text{H}_2\ \sigma_g$ , and M (in plane)  $np$  orbitals. The M inner-shell orbitals are not explicitly identified in this abbreviated notation. For the  $\text{MH}$  product molecule,  $1a_1$ ,  $2a_1$ , and  $1b_2$  denote the M-H  $\sigma$ ,  $\sigma^*$ , and  $\sigma$  orbitals, respectively. For the  $\text{MH} + \text{H}$  products,  $\sigma_{\text{MH}}$  labels the M-H bonding  $\sigma$  orbital,  $\sigma_{\text{M}}$  the M-centered non-bonding orbital, and  $\sigma_{\text{H}}$  the H-atom  $1s$  orbital.

Both of the above dominant configurations of the  $\text{M} + \text{H}_2$  reactant and  $\text{MH}_2$  product are of  $^1\text{A}_1$  symmetry, so they mix as one proceeds along the reaction path to produce the 'avoided crossing' which gives rise to the well known symmetry imposed activation barrier characteristic of such Woodward-Hoffmann forbidden reactions. For a  $\text{C}_{2v}$  symmetry preserving reaction path appropriate to the insertion of  $\text{B}^+$  into  $\text{H}_2$  to produce  $\text{HBH}^+$ , these correlations are described semi-quantitatively in Fig. 2.

#### 2. Low-Energy Excited State Configurations

The excited  $1,3P$  states of the M species, when interacting with  $H_2$  in  $C_{2v}$  symmetry, give rise to singlet and triplet states of  $A_1$ ,  $B_1$ , and  $B_2$  symmetry. The  $1,3B_2$  states possess the most attractive interactions because they allow M's in-plane np orbital of  $b_2$  symmetry to interact constructively with the  $H_2$  molecule's 'empty' antibonding  $\sigma_u$  orbital as shown in Fig. 3. The relative locations of these  $1,3B_2$  states along the insertion reaction's  $C_{2v}$  reaction path are also depicted in Fig. 2 (with the triplet states lying below the singlets).

## B. Implications for Reactivity

The fact that the  $1A_1$  ground state surface is either intersected or closely approached by the  $1,3B_2$  surfaces has important consequences for the insertion reaction under discussion. In particular, collisions entering the region where the  $1A_1$  and  $1B_2$  surfaces are close in energy may 'hop' from the  $ns^2 1A_1$  entrance-channel surface to the  $1B_2$  surface if the collision occurs with some degree of asymmetry. Collisions that occur slightly away from  $C_{2v}$  symmetry will experience weak coupling of the  $1A_1$  and  $1B_2$  surfaces (which are both of  $1A'$  symmetry in the lower  $C_s$  point group). The point is that any loss of  $C_{2v}$  symmetry permits the  $1A_1$  and  $1B_2$  states to mix, thereby allowing reactants to move onto the  $1B_2$  surface, which, in  $C_s$  symmetry, correlates to  $MH(2\Sigma) + H$  products. Of course, if any appreciable spin-orbit coupling is operative, transitions to the  $3B_2$  surface, which also correlates directly to the  $MH(2\Sigma) + H$  products, can also occur. It is through such surface 'hoppings' that the  $MH + H$  channel is accessed when the reaction begins with ground-state M and  $H_2$  species.

## C. Reaction Path "Shape"

A somewhat more quantitative view of the  $C_{2v}$  ground-state energy surface appropriate to these 'insertion' reactions is provided by Fig. 1 for the *ab initio* calculated  $1A_1$  surface of  $Be(1S) + H_2 \Rightarrow HBeH(X 1\Sigma_g)$ . This surface and others of this  $M(ns^2; 1S) + H_2 \Rightarrow HMH(1\Sigma_g)$  family are characterized by potential energy landscapes along which:

- The  $M + H_2$  entrance channel is very 'straight' (i.e., the reaction coordinate is dominated by M-to- $H_2$  relative motion with very little H-H displacement) and has very large positive curvature transverse to the reaction coordinate (i.e., the H-H bond remains intact and is very 'stiff').
- Once a critical M-to- $H_2$  distance is reached, the reaction coordinate undergoes a sudden change to become dominated by H-H stretching with much less M-to- $H_2$  movement.
- Further along the reaction path, a  $C_{2v}$  transition state is reached that lies more than 2 eV above<sup>1</sup> the energy of the  $M + H_2$  reactants and even above the energy of the  $MH + H$  fragments that could be formed if  $C_{2v}$  symmetry were not (artificially) enforced.
- Between the point where the reaction path acquires negative curvature along its 'uphill' coordinate and the  $C_{2v}$  - constrained transition state, a region appears within which negative curvature also exists along the asymmetric ( $b_2$ ) distortion. Because of the constraint to  $C_{2v}$  symmetry, the force (i.e., the energy gradient) along this  $b_2$  direction vanishes identically. The appearance of negative curvature along a direction transverse to the reaction coordinate indicates that a lower-energy path can be found if

one moves away from the  $C_{2v}$  geometry along this asymmetric direction. In the above cases, doing so eventually leads to formation of ground-state MH + H products. The negative curvature on the  $^1A_1$  surface along the  $b_2$  direction is a signal that a  $^1B_2$  surface is in close proximity; it does not mean that an intersection with a  $^1B_2$  surface is taking place, but that such a surface is energetically nearby. It is in this region of the surface that one must break  $C_{2v}$  symmetry in search of the true, lowest-energy, transition state.

e. If  $C_{2v}$  symmetry constraints are kept operative, movement along the  $b_2$  asymmetric mode will not occur, and the reaction coordinate will evolve smoothly to and beyond the  $C_{2v}$  - constrained transition state mentioned above.

f. Beyond this  $C_{2v}$  transition state, the reaction coordinate eventually develops positive curvature as the linear HMH( $^1\Sigma_g$ ) geometry is approached.

#### D. Why Study $B^+(^1S) + H_2$ ?

The present work is aimed at extending the investigations described above in at least two aspects: (i) to include a positive metal ion (but still with a closed-shell  $^1S$  ground electronic state) as the reactive species so any effects caused by ion-molecule interactions can be examined, and (ii) to investigate reaction paths that are not  $C_{2v}$  - preserving so as to permit the MH + H product channel to be explored. We chose  $B^+(^1S)$  as the positive ion because: (i) it is isoelectronic with Be( $^1S$ ) which we examined earlier (and thus similarities and differences between the Be and  $B^+$  cases are of interest), (ii) it allows highly accurate calculations to be performed with reasonable effort, and (iii) experimental guided ion beam and other data<sup>3a,3d</sup> giving the cross-section for  $BH^+$  production as a function of  $B^+$  kinetic energy are available and in need of theoretical interpretation.

## II. Computational Methods

### A. Basis Sets

The basis set for the H atoms consists of the Dunning augmented correlation consistent (cc) polarized valence triple-zeta (p-VTZ) [5s2p1d| 3s2p1d] set<sup>4</sup> of functions. For the  $B^+$  ion, the Dunning [10s5p2d| 4s3p2d] augmented cc p-VTZ basis set was used. A total of 55 contracted Gaussian-type basis functions resulted.

### B. Electronic Configurations and Wavefunctions

Both multiconfigurational self-consistent field (MCSCF) and coupled-cluster methods were used to treat correlations among the four valence electrons of the  $BHH^+$  system. In particular, the CCSD(T) variant<sup>5</sup> of the coupled-cluster approach<sup>6</sup>, which includes all single and double excitations in a fully correct manner and treats triple excitations by approximate non-iterative means, was employed.

The discussion of Sec. I makes it clear that no single electronic configuration can describe even the ground state of this system throughout the  $C_{2v}$  or  $C_s$  reaction paths. For this reason, multiconfigurational methods were required. In the MCSCF calculations, the four valence electrons were distributed, in all ways consistent with overall spatial and spin symmetry, among 6 valence orbitals. In the  $C_{2v}$  calculations, 4 of these orbitals were of  $a_1$  symmetry, 1 was of  $b_2$  symmetry, and 1 was of  $b_1$  symmetry. In  $C_s$  symmetry, there were 5 of  $a'$  symmetry and 1 of  $a''$  symmetry. The two  $B^+$  1s electrons

were constrained to occupy a single  $a_1$  or  $a'$  core orbital in all of the electronic configurations generated. This process generated 41 electronic configurations of  $1A_1$  symmetry in the  $C_{2v}$  point group and 65 of  $1A'$  symmetry in the  $C_s$  point group.

The above MCSCF calculations were employed, along with our Utah MESSKit<sup>7</sup> analytical energy derivative and potential energy surface 'walking' algorithms<sup>8</sup> to find and characterize (via geometry and local harmonic vibrational frequencies) the local minima, transition states, and reaction paths discussed below. Near each such point, the CCSD(T) method was used to evaluate the total correlation energies at a more accurate level; finite difference methods were also employed within the CCSD(T) approach to refine the predicted geometry of each such point on the surface.

### III. Findings and Comparison to Guided Ion Beam Results

As detailed in Table I and described qualitatively in Figs. 2 and 4, we find the potential energy surface for  $B^+(1S) + H_2 \Rightarrow BH^+(2\Sigma) + H$  to possess most of the features that are expected from the discussion in Sec. I. Although there are differences that might have been expected because of the additional long-range ion-molecule interactions that are operative in this case, we find such affects to be quite small in this case. Our primary findings are summarized as follows:

a. A weakly bound  $B^+ \cdots H_2$  complex lies  $1143 \text{ cm}^{-1}$  below the  $B^+ + H_2$  reactant energy. When zero-point corrected, this complex is stable by only  $855 \text{ cm}^{-1}$ . The complex has a triangular  $C_{2v}$  equilibrium structure in which the H-H internuclear distance is only slightly distorted from that of  $H_2$ ; the B-H distance (ca.  $2.6 \text{ \AA}$ ) is much longer than the covalent bond length in  $BH^+$  ( $1.2 \text{ \AA}$ ). Further along the reaction coordinate, one finds a 'straight and narrow' reaction path characterized by stronger and stronger  $B^+$ -to- $H_2$  inter-reactant forces but very small distortion of the H-H bond length or the H-H vibrational frequency. The very restricted range of geometries (i.e., the narrowness) of this entrance channel and its lack of 'curvature' coupling  $B^+$ -to- $H_2$  translational energy to H-H vibrational energy would be expected to produce clear signatures in the  $B^+ + H_2 \Rightarrow BH^+ + H$  experimental data.

b. As the  $B^+$  ion approaches the  $H_2$  molecule from very long range (e.g.,  $R = 25 \text{ \AA}$  or further), the charge-quadupole interaction (which varies as  $R^{-3}$ ) favors the 'T-shaped'  $C_{2v}$  approach which eventually produces the above straight and narrow reaction path. The permanent quadupole moment of  $H_2$  attracts positive ions to the internuclear regions and repels positive ions from positions along the H-H axis at long range. As one moves to smaller  $R$  values, the charge-induced dipole interaction (which varies as  $R^{-4}$ ) comes into play. This factor favors approach of a positive (or negative) ion along the H-H axis (because  $\alpha_{||} = 0.934 \text{ \AA}^3 > \alpha_{\perp} = 0.718 \text{ \AA}^3$ ). Although these electrostatic and induced interactions are dominant at very long range, we find that by the time the  $B^+$  is close enough to the  $H_2$  molecule to experience interaction energies of the order of a few kcal/mol, the energetically favored approach corresponds to a T-shaped  $C_{2v}$  structure. Although a colinear approach path may have been expected to be more favorable for larger  $R$  values, we find that the linear structure becomes unstable with respect to bending distortion even at rather large  $R$  values. As a result, the reaction path 'bends' toward the  $C_{2v}$  path which it then follows throughout the remainder of the  $B^+$  to  $H_2$  approach.

c. The  $B^+ + H_2 \Rightarrow BH^+ + H$  reaction is predicted to be endoergic by  $21,318\text{cm}^{-1}$  ( $20,497\text{cm}^{-1}$  when zero-point corrected). In the guided ion beam experiments<sup>3a</sup>, no flux of  $BH^+$  product ions are detected when  $B^+$  ions collide with  $H_2$  with kinetic energies at or slightly above this threshold; this has been used to infer that an additional activation barrier is present.

d. As one proceeds along the straight and narrow entrance channel starting from the  $B^+ + H_2$  species (along which  $C_{2v}$  symmetry obtains even though not enforced), a geometry is reached at which the asymmetric distortion mode (of  $b_2$  symmetry) develops negative curvature. This occurs at an energy of

$-25.341096$  Hartree,  $23,100\text{cm}^{-1}$  above the  $B^+ + H_2$  reactants; the geometry where this occurs has an HH distance of  $1.305\text{Å}$  and a BH distance of  $1.481\text{Å}$ . From here, distortion along the asymmetric mode leads to a transition state that lies below the  $C_{2v}$ -constrained transition state. The resulting  $C_s$  transition state structure possesses one 'long' B-H distance ( $r_{BH} = 1.765\text{Å}$ ), one 'short' B-H distance ( $r_{BH} = 1.251\text{Å}$ ) and an essentially 'broken' H-H bond ( $r_{HH} = 1.516\text{Å}$ ). Its energy is  $23,518\text{cm}^{-1}$  above the  $B^+ + H_2$  asymptote; when zero-point corrected, this point lies  $22,528\text{cm}^{-1}$  above  $B^+ + H_2$ . This critical point lies  $2031\text{cm}^{-1}$  or ca.  $0.25\text{eV}$  above the thermodynamic reaction threshold. This energy gap corresponds approximately to where the guided ion beam experiments first detect production of  $BH^+$  product ions.

e. A geometrically stable linear  $HBH^+(^1\Sigma)$  species is found to lie  $20,892\text{cm}^{-1}$  ( $19,259\text{cm}^{-1}$  when zero-point corrected) below  $B^+ + H_2$ . This species lies on the ground state  $^1A_1$  potential energy surface and correlates with the  $B^+(^1S) + H_2$  reactants when  $C_{2v}$  symmetry is enforced. Its BH bond length ( $r_{BH} = 1.173\text{Å}$ ) is only slightly longer than that in  $BH^+$  ( $1.2\text{Å}$ ).

f. In the absence of enforced  $C_{2v}$  symmetry, the  $^1A_1$  and  $^1B_2$  surfaces of Fig. 2 are of the same ( $^1A'$ ) symmetry, and can therefore couple to produce 'avoided crossings'. As a result of these interactions, the ground-state  $B^+(^1S) + H_2$  reactants can now correlate directly to the  $BH^+(^2\Sigma) + H$  products as summarized in the  $C_s$ -symmetry correlation diagram of Fig. 4.

#### IV. Discussion of Results and Summary

Many of the features observed for the  $B^+ + H_2$  surface(s) are remarkably similar to those found earlier for  $Be + H_2$ . In Fig. 5 we summarize the relative energies of the reactants, transition states, and products that arise in these two systems; in both cases, all energies are defined relative to the ground state of the  $M + H_2$  reactants.

The energy of the  $BeH_2^\ddagger$  transition state corresponds to  $C_{2v}$  symmetry although  $C_s$  symmetry was explored in these earlier calculations. As  $Be$  approaches  $H_2$ , the reaction path preserves  $C_{2v}$  symmetry and leads to the transition state shown in Fig. 5, at which the curvature along the asymmetric  $b_2$  distortion mode is positive. Past this transition state, along the way to the linear  $HBeH$  geometry, a state of  $^1B_2$  symmetry crosses the  $^1A_1$  surface. At this point, the curvature along the  $b_2$  mode is negative. As a

result, the reaction path moves away from  $C_{2v}$  symmetry and produces  $BeH + H$  products.

It may be somewhat surprising that, although the  $^3P$  and  $^1P$  excited states of  $B^+$  lie considerably higher than the corresponding  $^3,^1P$  states of  $Be$  (because of the higher nuclear charge of  $B^+$ ), the relative energies of the transition states,  $MH + H$ , and  $HMH$  species are rather similar. It should be noted that, because the  $^1,^3P$  states of  $B^+$  lie considerably higher than those of  $Be$ , the intersections of the resultant  $^1,^3B_2$  states with the  $^1A_1$  ground state are somewhat different for  $B^+$  and  $Be$ . In particular, both of the  $^1,^3B_2$  states of  $BeH_2$  intersect the  $^1A_1$  state near the  $C_{2v}$  transition state. However, it appears that the  $^1B_2$  state of  $BH_2^+$  does not intersect the  $^1A_1$  state as one proceeds along the reaction path toward the transition state (although it certainly couples strongly to it to produce the negative curvature along the  $b_2$  mode).

To explore such differences and similarities further, it is interesting to speculate about another isoelectronic system:  $Li^- + H_2 \Rightarrow LiH^- + H, HLiH^-$ . Using the known<sup>9</sup> electron affinities of  $Li$  and of  $LiH$ , as well as the  $LiH$  and  $H_2$  bond energies, one finds that  $LiH^- + H$  should lie  $19,100\text{ cm}^{-1}$  above  $Li^- + H_2$ . This energy difference is remarkably close to those for  $B^+ + H_2 \Rightarrow BH^+ + H$  and  $Be + H_2 \Rightarrow BeH + H$ . The energies of the  $HLiH^-$  species and of the  $C_{2v}$  or  $C_s$  transition states for the  $Li^- + H_2$  reaction are not yet known, so further comparisons can not be made.

Major differences between the  $Li^-$  case and those for  $B^+$  and  $Be$  involve the location of the  $^3,^1P$  excited states. For  $B^+$  and  $Be$ , the lowest of these states, the  $^3P$  state, lies  $37,300\text{ cm}^{-1}$  and  $22,000\text{ cm}^{-1}$ , respectively, above the  $^1S$  ground state. For  $Li^-$ , the  $^3P$  state lies higher in energy than  $Li$  (plus a free electron) and hence is metastable with respect to autodetachment. In particular, the  $^3P$  and  $^1P$  states are believed to lie between  $5000$  and  $10,000\text{ cm}^{-1}$  and between  $12,000$  and  $13,000\text{ cm}^{-1}$  above the  $^1S$  state, while the  $Li^-$  electron detachment energy is only  $5000\text{ cm}^{-1}$ . For these reasons, the intersection of the  $^1A_1$  ground state  $C_{2v}$  surface for  $Li^- + H_2$  by the excited  $^1B_2$  surface is expected to occur at much lower energy than in the  $B^+$  and  $Be$  cases. Moreover, the  $^2A_1$  surface corresponding to the autodetached  $Li + H_2$  species is also expected to come into play at low collision energies. Therefore, qualitatively different behavior is expected both in the low-energy potential surfaces of  $Li^- + H_2$  and in the guided ion beam experiments studying  $Li^-$  collisions with  $H_2$ . It is our intention to explore this interesting case in the near future.

Before closing, it should be mentioned that there are interesting aspects of the  $B^+ + H_2$  potential energy surfaces that were not addressed here because of our emphasis on the lowest singlet-state potential. In particular, the location of the  $^3B_2$  surface in the neighborhood of the singlet state's  $C_s$  transition state is of substantial importance to a full interpretation of the  $B^+ + H_2$  reactivity data. If transitions to the  $^1B_2$  surface play an important role, transitions to the corresponding triplet surface will also be operative. The latter events may occur with reduced probability because of the need for singlet-triplet coupling, but they will occur at lower energy because the  $^3B_2$  state lies below the  $^1B_2$  state.

Finally, in this work emphasis has been placed on the reaction path as it enters the 'straight and narrow' channel of  $C_{2v}$  symmetry; little has been said of colinear  $M-HH$  geometries. Hurst has shown that the linear approach does not lead to a lower-energy

path to the formation of  $BH^+(^2\Sigma) + H$ , and our data confirms that the energetically favored approach evolves into the  $C_{2v}$  geometry once the  $B^+$  and  $H_2$  begin to interact via chemical valence forces.

### **Acknowledgments**

This work was supported in part by the Office of Naval Research and by NSF Grant #CHE8814765. We acknowledge our colleague, Prof. P. B. Armentrout, for stimulating our interest in this particular system. We thank the Utah Supercomputer Institute for staff and computer resources.

## References:

1. D. O'Neal, H. Taylor, and J. Simons, *J. Phys. Chem.* **88**, 1510 (1984).
2. N. Adams, W. H. Breckenridge, and J. Simons, *Chem. Phys.* **56**, 327 (1981).
- 3a. P. B. Armentrout, *Inter. Rev. Phys. Chem.* **9**, 115 (1990); J. L. Elkind and P. B. Armentrout (unpublished results); S. A. Ruatta, L. Hanley, and S. L. Anderson, *J. Chem. Phys.* **91**, 226 (1989);
- 3b. P. Rosmus and R. Klein, Thesis by Klein, University of Frankfurt (1984).
- 3c. F. Schneider, L. Zülicke, R. Polak, and J. Vojtik, *Chem. Phys. Letts.* **105**, 608 (1984).
- 3d. K. C. Lin, H. P. Watkins, R. J. Cotter, and W. S. Koski, *J. Chem. Phys.* **56**, 1003 (1974); S. A. Ruatta, L. Hanley, and S. L. Anderson, *J. Chem. Phys.* **91**, 226 (1989).
4. T. Dunning, *J. Chem. Phys.* **90**, 1007 (1989).
5. K. Raghavachari, G. W. Trucks, J. A. Pople, and M. Head-Gordon, *Chem. Phys. Lett.*, **157**, 479 (1989).
6. J. Cizek, *J. Chem. Phys.* **45**, 4256 (1966); *Advan. Chem. Phys.* **14**, 35 (1969). J. Cizek, and J. Paldus, *Intern. J. Quantum Chem.* **5**, 359 (1971). R. J. Bartlett, *J. Phys. Chem.*, **93**, 1697 (1989) for a recent comprehensive review of developments in this field.
7. The Utah MESS-KIT is a suite of highly modular codes that were programmed in-house to give a variety of electronic structure functionalities by J.A. Nichols, M.R. Hoffmann, R.A. Kendall, H.L. Taylor, D.W. O'Neal, E. Earl, R. Hernandez, M. Gutowski, J.Boatz, K. Bak, J. Anchell, X. Wang, M. Feyereisen, and J. Simons.
8. J. Nichols, H. Taylor, P. Schmidt and J. Simons, *J. Chem. Phys.* **92**, 340 (1990); J. Simons, P. Jørgensen, H. Taylor, and J. Ozment, *J. Phys. Chem.* **87**, 2745 (1983); D. O'Neal, H. Taylor, and J. Simons, *J. Phys. Chem.* **88**, 1510 (1984); A. Banerjee, N. Adams, J. Simons, and R. Shepard, *J. Phys. Chem.* **89**, 52 (1985); H. Taylor and J. Simons, *J. Phys. Chem.* **89**, 684 (1985); C. J. Cerjan and W. H. Miller, *J. Chem. Phys.*, **75**, 2800 (1981); J. Baker, *J. Comp. Chem.* **9**(5), 465 (1988); J. Baker, *J. Comp. Chem.* **7**(4), 385 (1986).
9. The EA of Li is 0.62 eV (H. Hotop and W. C. Lineberger, *J. Phys. Chem. Ref. Data*, **14**, 731 (1985); the EA of LiH is 0.3 eV (K. M. Griffing, J. Kenney, J. Simons, and K. D. Jordan, *J. Chem. Phys.* **63**, 4073 (1975).
10. D. M. Hurst, *Chem. Phys. Letters* **95**, 591 (1983).

Table I. Total and Relative Energies, Geometries, and Vibrational Frequencies for Species Along the  $B^+ + H_2 \Rightarrow BH^+ + H$  Reaction Path<sup>a</sup>

| Species                          | Method Used                 | Electronic Energy (Hartrees)           | Optimized Geometry (Å)   | MCSCF Frequencies <sup>c</sup> / Zero Point Energies (cm <sup>-1</sup> ) | Relative Energies (cm <sup>-1</sup> ) <sup>b</sup> |
|----------------------------------|-----------------------------|--|--|--|--|
| $B^+(^1S) + H_2$                 | MCSCF<br>CCSD(T)            | -25.446357<br>-25.468865               | $r_{HH} = 0.755$<br>$r_{HH} = 0.734$   | 4224/2112  | 0  |
| $BH_2^+ C_{2v}$ complex          | MCSCF<br>CCSD(T)            | -25.468239<br>-25.474069               | $r_{HH} = 0.762$ ;<br>$r_{BH} = 2.605$<br>$r_{HH} = 0.743$ ;<br>$r_{BH} = 2.605$ | 230 ( $a_1$ ),<br>437 ( $b_2$ ),<br>4133 ( $a_1$ )/<br>2400              | -1143  |
| $BH_2^+ C_{2v}$ transition state | MCSCF<br>CCSD(T)            | -25.322627<br>-25.352230               | $r_{HH} = 1.396$ ;<br>$r_{BH} = 1.411$   | 4512i ( $a_1$ ),<br>1279 ( $a_1$ ),<br>3424i ( $b_2$ ) <sup>d</sup>      | 25,595   |
| $HBH^+(^1\Sigma)$                | MCSCF<br>CCSD(T)<br>CCSD(T) | -25.524859<br>-25.563931<br>-25.564067 | $r_{BH} = 1.183$<br>$r_{BH} = 1.172$<br>$r_{BH} = 1.173$                         | 2911 ( $a_1$ ),<br>2632 ( $b_2$ ),<br>973<br>(bending)/<br>3745          | -20,892  |
| $BH_2^+ C_s$ transition state    | MCSCF<br>CCSD(T)            | -25.332540<br>-25.361695               | $r_{HH} = 1.516$<br>$r_{BH} = 1.765$<br>$r_{BH} = 1.251$                         | 2840i, small <sup>e</sup> ,<br>2087/ ca.<br>1050                         | 23,518   |
| $BH^+(^2\Sigma) + H$             | MCSCF<br>CCSD(T)            | -25.351373<br>-25.371722               | $r_{BH} = 1.199$<br>$r_{BH} = 1.198$   | 2582/<br>1291  | 21,318   |
| $BHH^+$ linear complex           | MCSCF<br>CCSD(T)<br>CCSD(T) | -25.446663<br>-25.469942<br>-25.488630 | $r_{HH} = 0.756$<br>$r_{BH} = 2.729$<br>$r_{HH} = 0.702$<br>$r_{BH} = 2.865$     | 112, 4202,<br>303i<br>(bending) <sup>d</sup><br>/2157                    | -4337  |

a. Where separate geometry optimizations were carried out at the MCSCF and CCSD(T) levels, two sets of geometries are reported. In all cases, the MCSCF geometry is listed first, and the CCSD(T) geometry appears second. Where geometry optimization could not be carried out at the CCSD(T) level, the CCSD(T) energies were computed at the MCSCF geometries.

b. In all cases, only the CCSD(T) energies are used because they represent our best values. They are given relative to the  $B^+ + H_2$  reactants. These are electronic energies, and thus do not include zero-point corrections.

c. These local harmonic frequencies were obtained from the analytical second derivatives of the MCSCF energy at the MCSCF geometries.

d. It is not appropriate to compute zero point energies here because this is neither a true minimum nor transition state (i.e., more than one imaginary frequency appears).

e. The precise location of the  $C_s$  transition state was very difficult to determine. See text for further discussion.

## Figure Captions

Figure 1. Two-dimensional contour plot of the ground-state  $^1A_1$  potential energy surface for the  $C_{2v}$  insertion of  $Be(^1S)$  into  $H_2$  to produce linear  $HBeH(^1\Sigma)$ . The contour spacings represent approximately  $5,000\text{ cm}^{-1}$  in energy. The labels a-d, f refer to the geometrical points discussed in Sec. I.C. Along the vertical axis is the distance from the  $B^+$  to the center of the H-H bond; the horizontal axis labels the H-H distance.

Figure 2. Configuration correlation diagram for  $C_{2v}$  insertion of  $B^+(^1S)$  into  $H_2$  to produce linear  $HBH^+$ . The energies are in units of  $1000\text{ cm}^{-1}$ . The  $1a_1$ ,  $2a_1$ , and  $1b_2$  orbitals correspond to the  $H_2\ \sigma_g$ ,  $B^+\ 2s$ , and  $B^+\ 2p$  (in plane) orbitals, respectively for the  $B^+ + H_2$  reactants. For the  $HBH^+$  product, the  $1a_1$  and  $1b_2$  orbitals are the two (symmetric and asymmetric)  $\sigma$  B-H bonding orbitals.

Figure 3. Constructive interaction between the in-plane M np orbital of  $b_2$  symmetry and the antibonding  $H_2\ \sigma_u$  orbital also of  $b_2$  symmetry.

Figure 4. Configuration correlation diagram for  $C_s$  insertion of  $B^+(^1S)$  into  $H_2$  to produce either linear  $HBH^+$  or  $BH^+(^2S) + H$ . The energies are in units of  $1000\text{ cm}^{-1}$ . The  $1a'$ ,  $2a'$ , and  $3a'$  orbitals correspond to the  $H_2\ \sigma_g$ ,  $B^+\ 2s$ , and  $B^+\ 2p$  (in plane) orbitals, respectively for the  $B^+ + H_2$  reactants. For the  $HBH^+$  product, the  $1a'$  and  $3a'$  orbitals are the two (symmetric and asymmetric)  $\sigma$  B-H bonding orbitals. For  $BH^+ + H$ ,  $1a'$  is the  $BH^+$   $\sigma$  bonding orbital,  $3a'$  is the  $BH^+$  non-bonding  $\sigma$  orbital, and  $2a'$  is the H atom  $1s$  orbital.

Figure 5. Energy diagram showing relative energies of  $M + H_2$ ,  $HMH$ ,  $MH + H$ , and transition states for the  $B^+ + H_2$  and  $Be + H_2$  cases. Also shown are the locations of the  $^1,^3P$  excited states of the  $B^+$  and  $Be$  species. All energies are in units of  $1000\text{ cm}^{-1}$ .

